catalysts

MDPI

Article

Synthesis of a Novel Magnetically Retrievable Nanocomposite with Au Nanocatalysts for Hydration Reaction

Xiaoxi Yu [1], Yingjie Dai [2], Youran Wu [2], Yunfeng Cheng [3,*] and Qingshan Zhao [1,*]

1 State Key Laboratory of Heavy Oil Processing, College of Chemical Engineering, China University of Petroleum (East China), Qingdao 266580, China; yuxiaoxi@upc.edu.cn
2 College of Petroleum Engineering, China University of Petroleum (East China), Qingdao 266580, China; upcdyj@126.com (Y.D.); upcwyr@126.com (Y.W.)
3 School of Chemical Engineering and Technology, Tianjin University, Tianjin 300072, China
* Correspondence: cyf_1006@163.com (Y.C.); qszhao@upc.edu.cn (Q.Z.)

Received: 9 September 2019; Accepted: 18 September 2019; Published: 22 September 2019

Abstract: Developing efficient catalysts with good recyclability is of great importance for its practical applications. In this study, a novel magnetically retrievable nanocomposite (Au-SiO_2@Fe_3O_4-RGO) was synthesized for catalyzing hydration reaction. Active Au nanoparticles are deposited on core-shell SiO_2@Fe_3O_4, which are further supported by a two-dimensional reduced graphene oxide (RGO) platform. The prepared Au-SiO_2@Fe_3O_4-RGO was proven to be efficient as well as recyclable. An excellent catalytic performance, with 97% yield towards the hydration of phenylacetylene, was achieved for the catalyst in dioxane. Remarkably, the catalyst can be readily recycled through magnetic separation and achieved superior catalyst recovery and stability after seven cycles without any metal leaching. This work provides a strategy to fabricate recyclable and durable catalysts for industrial applications.

Keywords: Au nanoparticles; RGO; magnetically retrievable; hydration reaction

1. Introduction

The hydration reactions are of great importance for the production of valuable carbonyl derivatives. The first group of catalysts applied for hydration reaction is mercury salts [1,2]. However, due to the high toxicity of Hg, such catalysts often bring about severe health and environmental problems. Non-Hg organometallic catalysts, especially Au-based catalysts [3,4], have emerged with excellent catalytic performances. In recent years, great efforts have been put on exploring the high activity as well as the preparation methods for Au-based catalysts [5–9]. For instance, a 100% benzene conversion was achieved for the Au-based catalyst [5]. Gold catalysts prepared by mechanochemical activation exhibited superior water–gas shift activity than those prepared with coprecipitation [6]. However, Au catalysts are costly and hard to be recovered from reaction systems. Consequently, heterogeneous catalysts are developed by incorporating Au active species on solid supports such as carbon and silica (SiO_2) [10]. Even though the heterogeneous catalysts can be separated using centrifugation or filtration for reuse, the loss of catalyst during separation is still inevitable, which limits the practical applications of these heterogeneous catalysts.

Recently, functionalized nanoparticle and especially magnetic nanoparticles (MNPs) have attracted much attention in a vast field including magnetic-targeting drug delivery, magnetic resonance imaging, and catalysis [11–13]. The large surface area together with special magnetic properties make MNPs ideal supports for catalysts to achieve convenient separation and reuse, avoiding serious deformation

or loss. For instance, Dong et al. synthesized magnetic Ni@Pd core-shell catalysts for the reduction of 4-nitrophenol [14]. The resulting Ni@Pd/KCC-1 could be easily recovered by magnetic force and reused six times. Other examples including magnetic-Pd catalysts for reducing of nitrobenzene water [15] as well as cobalt platform-Pt for hydrogenation reaction [16] were explored afterwards. Despite convenience in separation, MNPs often agglomerate into big clusters leading to a decrease in catalytic activities. To overcome this drawback, MNPs coated with SiO_2 composites are developed, and application of SiO_2 coated magnetic catalysts can be found in hydration reaction, hydrogenation reaction, Knoevenagel condensation reaction, and so on [17,18]. Still and all, the aggregative trend cannot be totally restrained. With a typical two-dimensional structure and large surface area, graphene-based materials provides versatile platforms for the immobilization of silica-coated magnetic catalysts to further improve their stability and dispersity.

Herein, a novel magnetically retrievable nanocomposite (Au-SiO_2@Fe_3O_4-RGO) was fabricated as an efficient and retrievable catalyst for hydration reaction. Active Au nanoparticles are deposited on core-shell SiO_2@Fe_3O_4, which are further supported by a two-dimensional reduced graphene oxide (RGO) platform. The prepared Au-SiO_2@Fe_3O_4-RGO composite was characterized by X-Ray diffraction (XRD), transmission electron microscopy (TEM), X-ray photoelectron spectroscopy (XPS), as well as inductively coupled plasma (ICP) to verify the hierarchical structure. The Au-SiO_2@Fe_3O_4-RGO showed excellent catalytic performance and superior reusability towards the hydration of phenylacetylene.

2. Results and Discussion

2.1. Characterization of Au-SiO_2@Fe_3O_4-RGO

The crystalline structure of the prepared Au-SiO_2@Fe_3O_4-RGO composite was primarily analyzed using XRD, as shown in Figure 1. The spectrum shows the specific diffraction peaks of Fe_3O_4 and Au, matching well with the standard pattern [19,20]. Interestingly, no diffraction peak of SiO_2 is observed, indicating that silica coated on the surface of Fe_3O_4 nanoparticles has an amorphous structure [21].

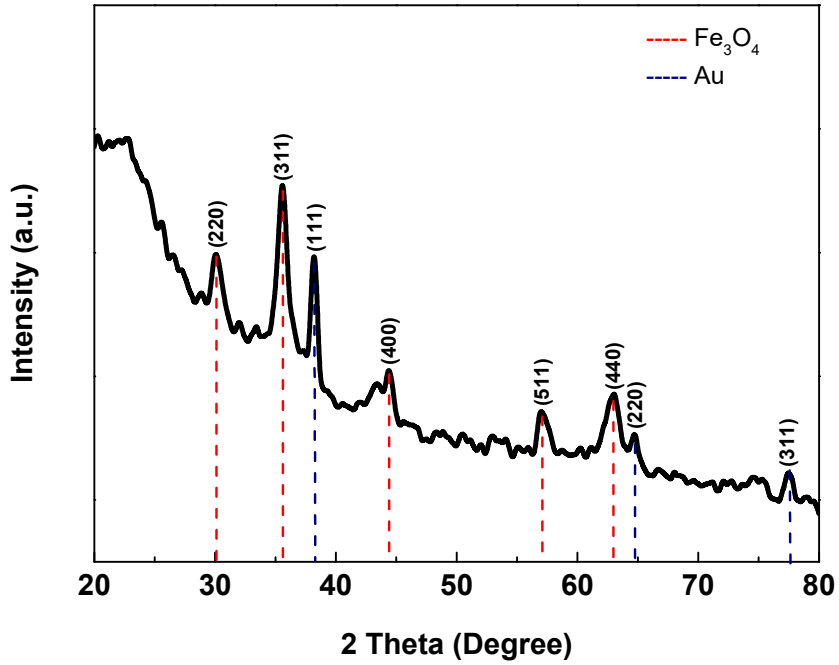

Figure 1. XRD patterns of Au-SiO_2@Fe_3O_4-RGO. Typical peaks of Au are marked with red dotted line, and typical peaks of Fe_3O_4 are marked with blue dotted line.

The morphology of the composites was observed with the assistance of TEM. Figure 2a shows the TEM image of SiO_2@Fe_3O_4-RGO composite. The surface of RGO is homogeneously and condensedly

decorated with Fe_3O_4 nanoparticles with an average diameter of about 15 nm, and no agglomerate was observed. It can be clearly seen that the nanoparticles on the surface are coated with a bright color layer. The typical core-shell structure suggests the surface coating of SiO_2 layer (about 4 nm) on the outside of the Fe_3O_4 core. Figure 2b displays the TEM image of the prepared Au-SiO_2@Fe_3O_4-RGO composite. Additional nanoparticles are further located around the surface of the core-shell structure, verifying the successful deposition of Au nanoparticles on the SiO_2@Fe_3O_4-RGO substrate. The Au nanoparticles are uniformly dispersed and show an average diameter of 7 nm.

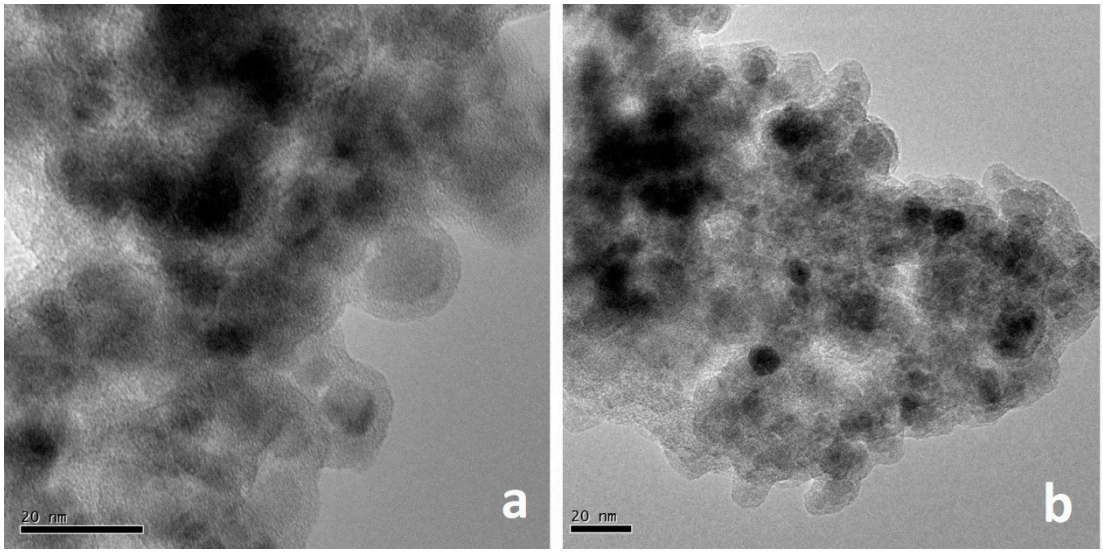

Figure 2. TEM images of composite, (**a**) shows SiO_2@Fe_3O_4-RGO and (**b**) shows Au-SiO_2@Fe_3O_4-RGO.

XPS analysis was further conducted to investigate the structural composition of Au-SiO_2@Fe_3O_4-RGO. As can be seen from the full range XPS spectrum in Figure 3a, the peaks at binding energies of 83.7 eV, 104.0 eV, 284.6 eV, 530.3 eV, and 711.3 eV correspond to the binding energies of Au $4f_{7/2}$, Si 2p, C 1s, O 1s, and Fe $2p_{1/2}$, respectively. This result further demonstrates the successful preparation of the Au-SiO_2@Fe_3O_4-RGO composite. Moreover, the Fe band is divided into two peaks at binding energies of 711.3 and 724.0 eV, which is consistent with the $2p_{3/2}$ and $2p_{1/2}$ binding energies of Fe_3O_4, in accordance with reported literatures (Figure 3b) [22,23]. In addition, the Si band was analyzed as well. As can be seen from Figure 3c, the Si 2p spectrum exhibits a characteristic band at 102.9 eV, standing for the binding energy of Si^{4+} 2p and signifying the existence of SiO_2 [22]. Two typical peaks at 83.7 and 87.1 eV are found in the Au 4f spectrum shown in Figure 3d, standing for the binding energy of Au (0) (Figure 3d) [24]. The lower binding energy acquired here may be attributed to the electron donor effect of the supporter. The negatively charged gold is beneficial to the adsorption of the phenylacetylene reactant, which further accelerates the reaction. Moreover, as can be seen from Figure 3e, the C 1s spectrum of GO are mainly composed of four peaks. The peak at 284.6 eV stands for the binding energy of C–C or C=C, the one at 286.5 eV corresponds to the binding energy of C–O from epoxy group, and the ones at 288.3 eV and 289.1 eV represent the existence of C=O and O–C=O from carboxyl group [25]. The Raw curve in Figure 3e overlaps with the Sum curve, indicating the spectrum was well-overfitted. As a contrast, compared with GO, the C–O–C and C–OH peaks at 286.7 eV in the C 1s XPS spectrum of Au-SiO_2@Fe_3O_4-RGO decreased remarkably, indicating the GO precursor was partially reduced to RGO during preparation (Figure 3f). The content of Au in the Au-SiO_2@Fe_3O_4-RGO composite was evaluated using ICP and found to be 0.31 mmol/g, close to the calculated value.

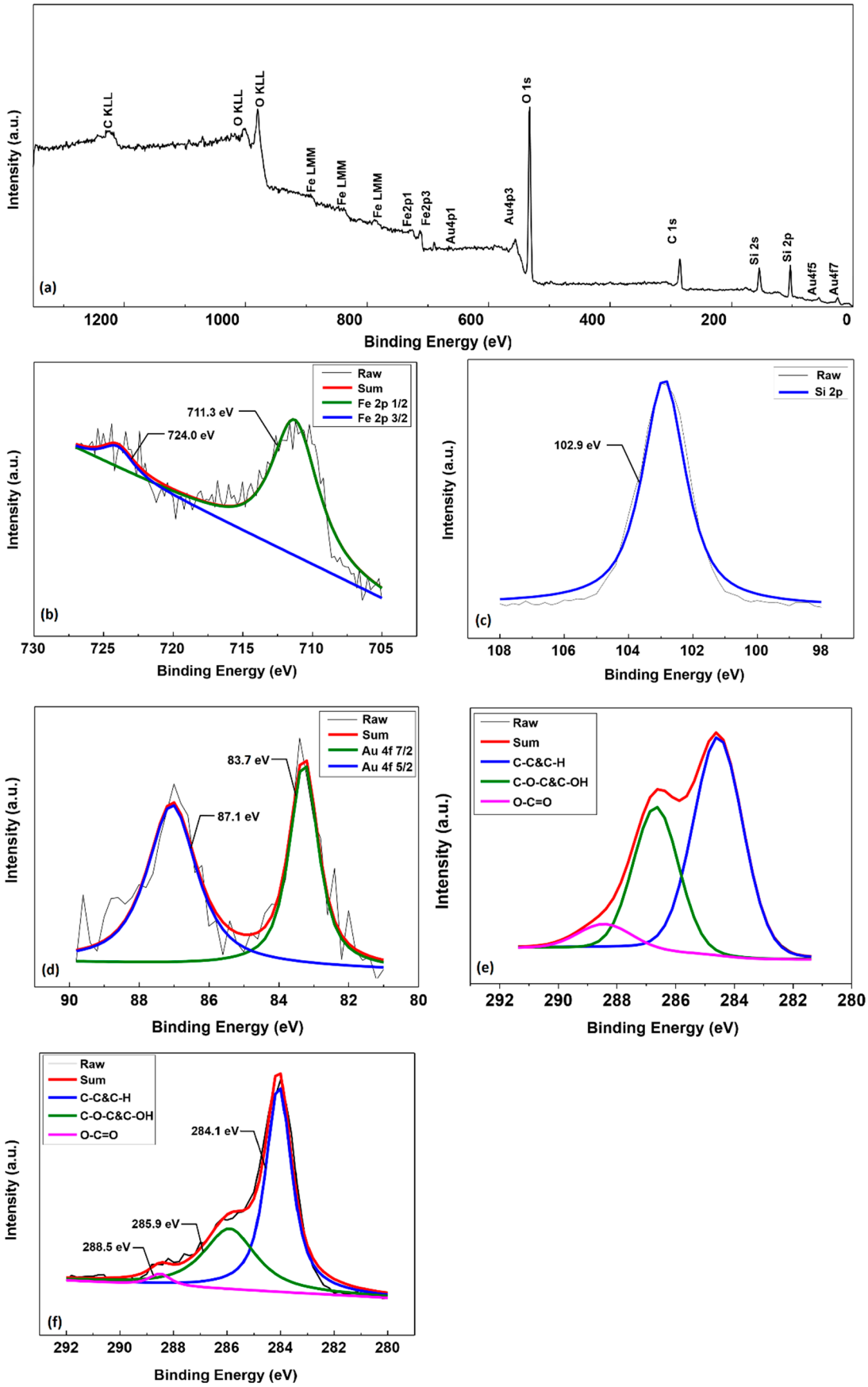

Figure 3. (**a**) Full range XPS spectrum of Au-SiO_2@Fe_3O_4-RGO, (**b**) Fe 2p, (**c**) Si 2p, and (**d**) Au 4f XPS spectra of Au-SiO_2@Fe_3O_4-RGO; C 1s XPS spectra of (**e**) GO and (**f**) Au-SiO_2@Fe_3O_4-RGO.

2.2. Catalytic Reaction

The catalytic performance of the Au-SiO_2@Fe_3O_4-RGO composite was examined with the hydration of phenylacetylene in dioxane. Table 1 summarizes the catalytic performance of the catalysts. Without any catalyst, a yield of only 9% was observed, meaning the necessity of an effective catalyst (Entry 1). Similarly, the SiO_2@Fe_3O_4-RGO catalyst without Au also showed a poor activity and resulted a yield of 10% (Entry 2). In contrast, the yield increased to 97 % for Au-SiO_2@Fe_3O_4-RGO, which demonstrates the catalytic activity of Au species for the proceeding of the hydration reaction (Entry 3). As a control, nonmagnetic Au–RGO was prepared and also displayed an excellent catalytic performance, achieving a yield of 95% under the same condition (Entry 4). To investigate the influence of solvent on the catalytic results, the reaction was further carried out in water other than dioxane (Entry 5). A slightly inferior performance (90% yield) was shown.

Table 1. Catalytic efficiencies towards the hydration of phenylacetylene [1].

Entry	Sample	Au (mmol/g)	Solvent	Yield (%) [2]
1	Blank	/	dioxane	9
2	SiO_2@Fe_3O_4–RGO	/	dioxane	10
3	Au–SiO_2@Fe_3O_4–RGO	0.31	dioxane	97
4	Au–RGO	0.36	dioxane	95
5	Au–SiO_2@Fe_3O4–RGO	0.31	H_2O	90

[1] General conditions: H_2O (0.5 mmol), phenylacetylene (0.25 mmol), solvent (dioxane or water 5 mL), and catalyst (3 mmol% Au) with oil bath (120 °C) for 8 h. [2] Calibrated yields determined by GC.

Considering the significance of the separation and durability of catalysts for industrial application, the reusability of the catalysts were systematically studied. As shown in Figure 4, when added into the reaction solution, the black Au-SiO_2@Fe_3O_4-RGO composite is uniformly dispersed, which is beneficial to the mass transfer in the reaction proceeding process. After the reaction, the black composite can be instantly attracted to the side with the assistance of a magnet within one minute, implying the convenient separation of the catalyst from the reaction system. The reusability of Au-SiO_2@Fe_3O_4-RGO was firstly investigated. As can be observed from Figure 5, the catalyst could be successfully recycled 7 times without any loss in activity and selectivity. Remarkably, in the cyclic reuse process, the catalyst showed nearly 100% recovery in the first runs owing to the excellent magnetism and afforded 95% recovery after 7 cycles. By contrast, for Au-RGO catalyst without magnetism (Figure 6), a significant loss in recovery was accompanied using centrifugation and got a recovery of 75% after 4 times. The leaching of Au-RGO catalyst resulted in simultaneously obvious decrease in the catalytic yield (82%).

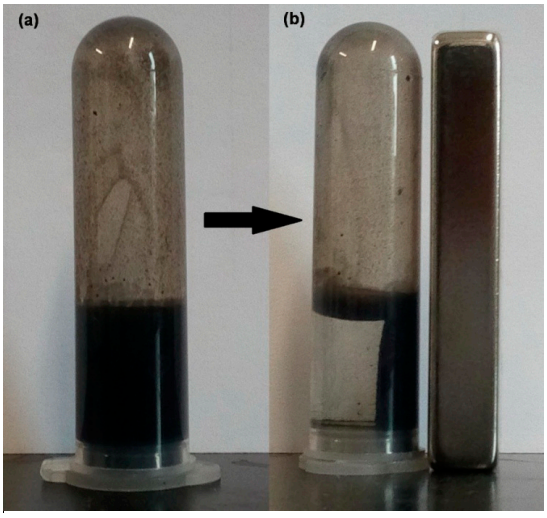

Figure 4. (**a**) Image of Au-SiO_2@Fe_3O_4-RGO suspension before the reaction. (**b**) Image of the reaction system with an additional magnet on the side after the reaction.

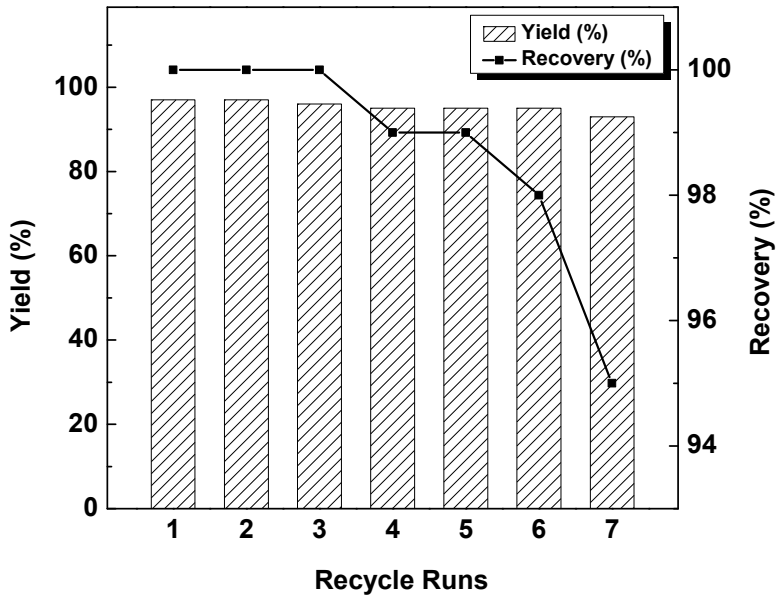

Figure 5. Catalyst recycling test in dioxane of Au-SiO_2@Fe_3O_4-RGO.

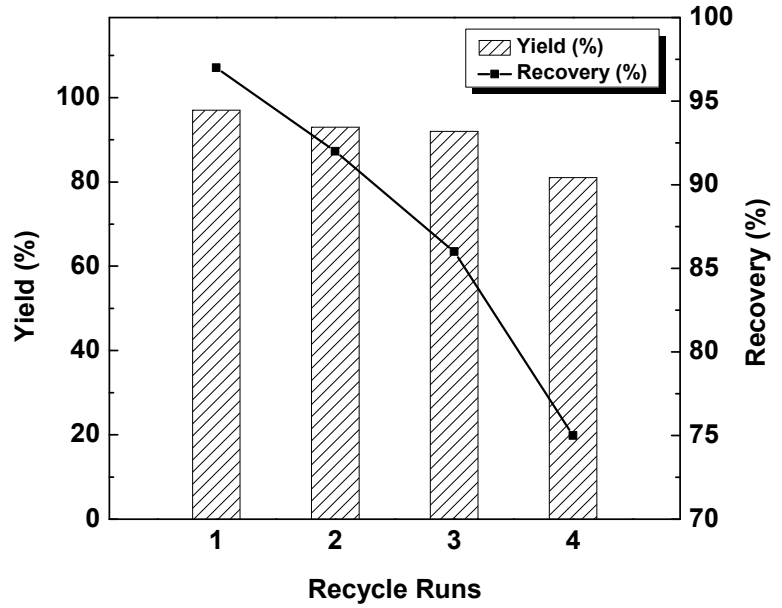

Figure 6. Catalyst recycling test in dioxane of Au-RGO.

Furthermore, when dissolved in water, Au-SiO_2@Fe_3O_4-RGO showed a relatively stable catalytic performance and slight activity decrease after 6 cycles. The recovery started to decrease after 2 cycles. Both yield and recovery are lower in the water solution compared with those in dioxane (Figure 7). This is probably because the prepared Au-SiO_2@Fe_3O_4-RGO has a good hydrophilicity and disperses better in the aqueous solution than in the dioxane solution. The catalyst is more difficult to retrieve in water, leading to a lower recovery. Therefore, dioxane is a favorable solvent, which leads to enhanced catalytic activity and recovery at the same time. In addition, to quantify the remaining residual catalyst in solution, ICP was applied to analyze the metal content in the solution after each reaction cycle. No signal of Au or Fe was traced, confirming the superior stability of Au-SiO_2@Fe_3O_4-RGO after the recycling.

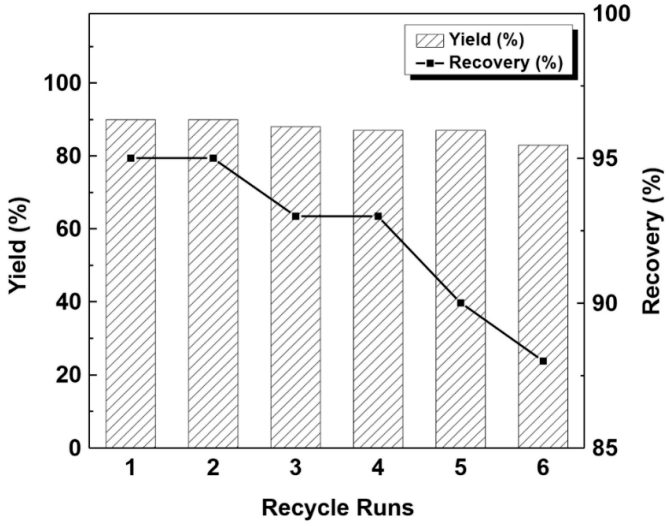

Figure 7. Catalyst recycling test in water of Au-SiO_2@Fe_3O_4-RGO.

3. Materials and Methods

3.1. Preparation of Fe_3O_4-RGO

Graphene oxide (GO) was prepared using a typical Hummers method [26]. Fe_3O_4-RGO was prepared using a coprecipitation method. An amount of 25 mL of the obtained GO solution was diluted to 150 mL with distilled water in a three-necked flask. The obtained suspension was ultrasonic bathed for 15 min to ensure it was evenly dispersed. The suspension was heated to 80 °C with magnetic stirring under nitrogen atmosphere. Then, 1.86 g ferric chloride ($FeCl_3 \cdot 6H_2O$, 6.8 mmol) and 0.96 g ferrous sulfate ($FeSO_4 \cdot 7H_2O$, 3.4 mmol) were injected to the GO suspension. Subsequently, 2 mL ammonia solution (25%) was added into the flask rapidly. The mixture was stirred for 45 min and cooled to room temperature. The resulting Fe_3O_4-RGO was washed successively with ultrapure water and ethanol, and dried with a vacuum oven.

3.2. Synthesis of Au-SiO_2@Fe_3O_4-RGO

A total of 350 mg of synthesized Fe_3O_4-RGO was dissolved in a solvent mixture of 320 mL ethanol and 80 mL water. A 12 mL 25% ammonia solution was added under continuous mechanical stirring. Subsequently, 1.2 mL of tetraethyl orthosilicate (TEOS) was added dropwise to the mixture. The reaction started immediately and lasted for 3 h at 40 °C. The resulting solid product (SiO_2@Fe_3O_4-RGO) was collected using a magnet and washed three times with water and ethanol, respectively.

A total of 500 mg of the synthesized SiO_2@Fe_3O_4-RGO was suspended in 200 mL distilled water for 10 min. Afterwards, 40 mL 0.1 M sodium dodecyl sulfate (SDS) solution followed with 3 mL 0.02 M chloroauric acid solution ($HAuCl_4$) was injected to the mixture. The mixture was heated under mechanical stirring with oil bath at 100 °C. After cooling to room temperature, the mixture was centrifuged three times and the pellet (Au-SiO_2@Fe_3O_4-RGO) was washed with distilled water to remove excess supernatant. The whole synthesis process is illustrated in Figure 8.

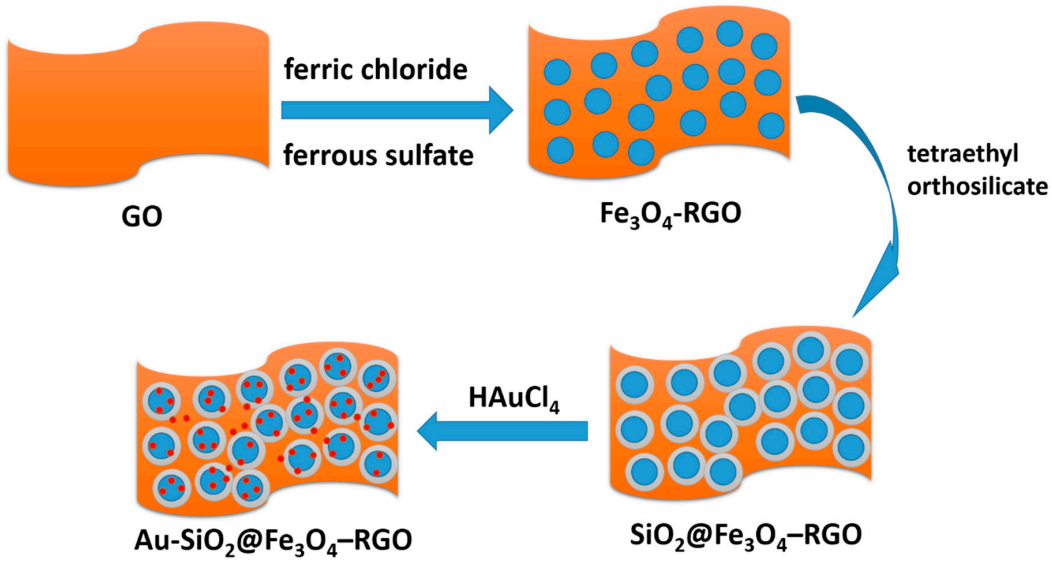

Figure 8. Illustration of the preparation of Au-SiO_2@Fe_3O_4-RGO.

3.3. Catalytic Hydration Reactions

Amounts of 0.25 mmol phenylacetylene, 0.5 mmoL distilled water, 1.0 mmoL sulfuric acid, and catalysts with 0.0025 mmoL Au were mixed in 5 mL solvent (dioxane or water). The mixture was then heated to 120 °C with oil bath and agitated for 8 h. After the reaction finished, samples were filtered and characterized using gas chromatography (GC). Identical reaction conditions were used for the recycling experiments. After reaction, the catalysts were recovered with a magnet, washed with ethanol and distilled water three times, and freeze-dried for reuse in the next run.

3.4. Characterizations

XRD was performed on a Bruker–Nonius D8 FOCUS diffractometer (Bruker, Karlsruhe, Germany). TEM images were recorded with a JEM-2100F transmission electron microscope (JEOL, Tokyo, Japan) operating at 200 kV. XPS measurements were carried out on a PHI 1600 spectrometer (Perkin–Elmer) (Perkin Elmer, Waltham, MA, USA). The content of Au in catalyst was analyzed using a Vista-MPX ICP (Varian, Palo Alto, CA, USA). The catalytic performance were evaluated by an Agilent 6890N GC (Agilent, Santa Clara, CA, USA) using the standard curve method.

4. Conclusions

A novel Au-SiO_2@Fe_3O_4-RGO composite was prepared by uniformly depositing Au NPs on the surface of SiO_2@Fe_3O_4-RGO plane. The catalyst was successfully prepared, as proved by XRD, TEM, XPS, and ICP. The prepared Au-SiO_2@Fe_3O_4-RGO showed excellent 97% yield towards hydration of phenylacetylene in dioxane and could be readily recycled for 7 with superior stability. This work provides a strategy to fabricate recyclable and durable catalysts for industrial applications.

Author Contributions: Conceptualization, Y.C. and Q.Z.; methodology, X.Y., Y.D., and Y.W.; writing—original draft preparation, X.Y.; writing—review and editing, Q.Z.

Funding: This research was financially supported by the Shandong Provincial Natural Science Foundation (No. ZR2019QB016, ZR2017BB085), China; the Fundamental Research Fund for the Central Universities (No. 18CX02015A, 18CX02146A), China; the National Natural Science Foundation of China (21706284).

Conflicts of Interest: The authors declare no conflict of interest.

References

1. Chapman, D.; Jenkins, W. LXIX.—The interaction of acetylene and mercuric chloride. *J. Chem. Soc. Trans.* **1919**, *115*, 847–849. [CrossRef]
2. Wang, S.; Miao, C.; Wang, W.; Lei, Z.; Sun, W. Hydration of terminal alkynes catalyzed by a water-soluble salen-Co(III) complex. *Chin. J. Catal.* **2014**, *35*, 1695–1700. [CrossRef]
3. Li, F.; Wang, N.; Lu, L.; Zhu, G. Regioselective hydration of terminal alkynes catalyzed by a neutral gold(I) complex [(IPr)AuCl] and one-pot synthesis of optically active secondary alcohols from terminal alkynes by the combination of [(IPr)AuCl] and Cp*RhCl[(R,R)-TsDPEN]. *J. Org. Chem.* **2015**, *80*, 3538–3546. [CrossRef] [PubMed]
4. Chen, T.; Cai, C. Catalytic hydration of alkynes to ketones by a salen–gold (III) complex. *Catal. Commun.* **2015**, *65*, 102–104. [CrossRef]
5. Ilieva, L.; Petrova, P.; Liotta, L.F.; Sobczak, J.W.; Lisowski, W.; Kaszkur, Z.; Munteanu, G.; Tabakova, T. Gold catalysts on Y-doped ceria supports for complete benzene oxidation. *Catalysts* **2016**, *6*, 99. [CrossRef]
6. Tabakova, T.; Ilieva, L.; Ivanov, I.; Zanell, R.; Sobczak, J.W.; Lisowski, W.; Kaszkur, Z.; Andreev, D. Influence of the preparation method and dopants nature on the WGS activity of gold catalysts supported on doped by transition metals ceria. *Appl. Catal. B Environ.* **2013**, *136–137*, 70–80. [CrossRef]
7. Wojcieszak, R.; Ferraz, C.P.; Sha, J.; Houda, S.; Rossi, L.M.; Paul, S. Advances in base-free oxidation of bio-based compounds on supported gold catalysts. *Catalysts* **2017**, *7*, 352. [CrossRef]
8. Tabakova, T.; Ivanov, I.; Karakirova, Y.; Karashanova, D.; Venezia, A.M.; Petrova, P.; Avdeev, G.; Kolentsova, E.; Ivanov, K. Promotional effect of gold on the WGS activity of alumina-supported copper-manganese mixed oxides. *Catalysts* **2018**, *8*, 563. [CrossRef]
9. Tabakova, T. Recent Advances in Design of Gold-Based Catalysts for H-2 Clean-Up Reactions. *Front. Chem.* **2019**, *7*, 517. [CrossRef]
10. Corma, A.; Garcia, H. Supported gold nanoparticles as catalysts for organic reactions. *Chem. Soc. Rev.* **2008**, *37*, 2096–2126. [CrossRef]
11. Sperling, R.; Parak, W. Surface modification, functionalization and bioconjugation of colloidal inorganic nanoparticles. *Phil. Trans. R. Soc. A* **2010**, *368*, 1333–1383. [CrossRef] [PubMed]
12. Wu, Y.; Wang, R.; Dai, C.; Xu, Y.; Yue, T.; Zhao, M. Precisely tailoring bubble morphology in microchannel by nanoparticles self-assembly. *Ind. Eng. Chem. Res.* **2019**, *58*, 3707–3713. [CrossRef]
13. Liu, F.; Laurent, S.; Fattahi, H.; Elst, L.; Muller, R. Superparamagnetic nanosystems based on iron oxide nanoparticles for biomedical imaging. *Nanomedicine* **2011**, *6*, 519–528. [CrossRef] [PubMed]
14. Liu, H.; Zhang, J.; Chen, X.; Du, X.; Zhang, J.; Liu, G.; Zhang, W. Application of iron oxide nanoparticles in glioma imaging and therapy: from bench to bedside. *Nanoscale* **2016**, *8*, 7808–7826. [CrossRef] [PubMed]
15. Dong, Z.; Le, X.; Dong, C.; Zhang, W.; Li, X.; Ma, J. Ni@Pd core–shell nanoparticles modified fibrous silica nanospheres as highly efficient and recoverable catalyst for reduction of 4-nitrophenol and hydrodechlorination of 4-chlorophenol. *Appl. Catal. B* **2015**, *162*, 372–380. [CrossRef]
16. Shokouhimehr, M.; Hong, K.; Lee, T.; Moon, C.; Hong, S.; Zhang, K.; Suh, J.; Choi, K.; Varma, R.; Jang, H. Magnetically retrievable nanocomposite adorned with Pd nanocatalysts: efficient reduction of nitroaromatics in aqueous media. *Green Chem.* **2018**, *20*, 3809–3817. [CrossRef]
17. Jun, C.; Park, Y.; Yeon, Y.; Choi, J.; Lee, W.; Ko, S.; Cheon, J. Demonstration of a magnetic and catalytic Co@Pt nanoparticle as a dual-function nanoplatform. *Chem. Commun.* **2006**, *15*, 1619–1621. [CrossRef]
18. Wei, S.; Wang, Q.; Zhu, J.; Sun, L.; Lin, H.; Guo, Z. Multifunctional composite core–shell nanoparticles. *Nanoscale* **2011**, *3*, 4474–4502. [CrossRef]
19. Li, J.; Zhang, S.; Chen, C.; Zhao, G.; Yang, X.; Li, J.; Wang, X. Removal of Cu(II) and Fulvic Acid by Graphene Oxide Nanosheets Decorated with Fe_3O_4 Nanoparticles. *ACS Appl. Mater. Inter.* **2012**, *4*, 4991–5000. [CrossRef]
20. Li, Z.; Wang, Y.; Ni, Y.; Kokot, S. Fluorescence analysis of 6-mercaptopurine with the use of a nano-composite consisting of BSA-capped Au nano-clusters and core–shell Fe_3O_4–SiO_2 nanoparticles. *Biosens. Bioelectron.* **2015**, *70*, 246–253. [CrossRef]
21. Yao, Y.; Miao, S.; Wang, S. Fabrication of Fe_3O_4/SiO_2 core/shell nanoparticles attached to graphene oxide and its use as an adsorbent. *Colloid Interf. Sci.* **2012**, *379*, 20–26. [CrossRef] [PubMed]

22. Wang, L.; Zhu, J.; Yang, H.; Wang, F.; Qin, Y.; Zhao, T.; Zhang, P. Fabrication of hierarchical graphene@Fe_3O_4@SiO_2@polyaniline quaternary composite and its improved electrochemical performance. *J. Alloy. Compd.* **2015**, *634*, 232–238. [CrossRef]
23. Zubir, N.; Yacou, C.; Motuzas, J.; Zhang, X.; Costa, J. Structural and functional investigation of graphene oxide–Fe_3O_4 nanocomposites for the heterogeneous Fenton-like reaction. *Sci. Rep.* **2014**, *4*, 101–104. [CrossRef]
24. Wang, Y.; Yu, J.; Xiao, W.; Li, Q. Microwave-assisted hydrothermal synthesis of graphene based Au–TiO_2 photocatalysts for efficient visible-light hydrogen production. *J. Mater. Chem. A* **2014**, *2*, 3847–3855. [CrossRef]
25. Zhao, Q.; Li, Y.; Liu, R.; Chen, A.; Zhang, G.; Zhang, F.; Fan, X. Enhanced hydrogenation of olefins and ketones with a ruthenium complex covalently anchored on graphene oxide. *J. Mater. Chem. A* **2013**, *1*, 15039–15045. [CrossRef]
26. Hummers, W.; Offeman, R. Preparation of Graphitic Oxide. *J. Am. Chem. Soc.* **1958**, *80*, 1339. [CrossRef]